Int. J. Solids Structures Vol. 24, No. 12, pp. 1205–1224, 1988
Printed in Great Britain.

0020-7683/88 $3.00 + .00

HYBRID MODELLING OF SEMI-INFINITE MEDIA

R. K. N. D. RAJAPAKSE and A. H. SHAH
Department of Civil Engineering, University of Manitoba, Winnipeg, Canada R3T 2N2

(*Received* 22 *April* 1987; *in revised form* 10 *June* 1988)

Abstract—An accurate and efficient hybrid formulation based on Lagrange's equations of motion is presented to solve geometrically axisymmetric problems associated with layered semi-infinite media under arbitrary loading. A near-field region containing all inhomogeneities is modelled using conventional finite elements. The contribution of the exterior semi-infinite domain to the equations of motion is represented by a surface integral defined over the finite element boundary. The integrand of this integral involves a matrix relationship between harmonics of nodal displacements and tractions at the finite element boundary. A boundary traction–displacement relationship for the exterior domain is established in terms of traction and displacement Green's functions for a uniform (undisturbed) half space. The present formulation guarantees a symmetric stiffness matrix for the entire system. Therefore, both direct and indirect versions of the boundary integral equation method can be used. The accuracy of the hybrid modelling algorithm is confirmed by solving a few elastostatic and elastodynamic boundary-value problems for which analytical solutions can be derived.

INTRODUCTION

An interesting class of problems in mechanics is associated with domains which are considered to be unbounded. In particular, theoretical idealizations adopted for analysis of three-dimensional problems encountered in geomechanics, seismology, composite materials, fracture mechanics, and non-destructive testing applications are based on models involving layered semi-infinite media. The interest in problems involving semi-infinite media may be traced back to the classical studies by Boussinesq (1885), Cerruti (1882), Lamb (1904), and Mindlin (1936), dealing with a point loading of a homogeneous half space. The majority of practical problems associated with semi-infinite media involves complicated geometries, boundary conditions, and non-homogeneous material compositions. An attempt to obtain an analytical solution to such a problem often leads to the solution of a mathematically intractable boundary-value problem.

Previous work

The application of the finite element method to the present class of problems is encountered with the fundamental problem of adopting a finite size model for a medium which is unbounded. Large size finite element models with elementary boundaries could circumvent this difficulty for static loading. However, as can be seen from the work of Muki and Dong (1980), the dimensions of such a finite element model have to be quite large and the solution is highly inefficient, especially when layered systems are considered. An attractive alternative to obtain better efficiency while preserving the accuracy was pioneered by Bettes (1977), Bettes and Zienkiewicz (1977), and Anderson and Ungless (1977), by introducing infinite elements to model the far-field domain of an unbounded homogeneous medium. The concept of infinite elements has been recently extended to elastostatic problems involving a multi-layered half space (Rajapakse and Karasudhi, 1985).

In the case of elastodynamic problems, finite element models with elementary boundaries violate the radiation conditions and lead to spurious solutions. Lysmer and Kuhlemeyer (1969) proposed to avoid reflection at the boundary of the finite element model by placing dashpots at nodal locations. This approach, known as the viscous boundary model, is strictly valid only for one-dimensional waves with normal incidence. Waas (1972) presented an accurate transmitting boundary for plane and axisymmetric problems of a layered stratum underlain by a rigid base. This algorithm was later extended to axisymmetric problems under arbitrary loading by Kausel *et al.* (1975). The concept of the infinite element has also been extended to elastodynamic problems (Chow and Smith, 1981; Medina and

Penzien, 1982; Rajapakse and Karasudhi, 1986) associated with a homogeneous elastic half space.

The global–local finite element method developed by Mote (1971) to study beam and plate vibration problems has recently been extended to study elastostatic and elastodynamic problems of unbounded media by Muki and Dong (1979, 1980), Dong (1981), Goetschel *et al.* (1982), and Avanessian *et al.* (1986a,b). For elastodynamic problems, the method relies on the use of wave function solutions for a full space, and this violates the traction free boundary conditions when applied to half space problems. The study by Avanessian *et al.* (1986a,b) proposes to achieve traction-free boundary conditions at the surface level for half space problems by imposing a set of integral constraints on tractions resulting from the full space solution at the surface level. The effectiveness and accuracy of this method to solve a variety of elastodynamic problems associated with an isotropic homogeneous half space has been demonstrated by Avanessian *et al.* (1986a,b). The disadvantage of this approach is the difficulty associated with its extension to layered systems, in particular, for elastodynamic problems.

During the last two decades, a considerable development has been reported (Cruse and Rizzo, 1975; Cruse *et al.*, 1985) in the application of the boundary integral equation method to solve a variety of boundary-value problems in mechanics. The pioneering work of Rizzo (1967) dealing with elastostatics and later work by Cruse and Rizzo (1968) and Cruse (1968) presented a systematic application of the boundary integral equation method to problems in elasticity. A recent article by Kobayashi (1984) presents a concise treatment of the application of the boundary integral equation method to elastodynamics and the study by Rizzo *et al.* (1985) considered the application to scattering and radiation problems involving a full space.

In recent years, some attention has been focused on the coupling of the finite element method and the boundary integral equation to solve more complicated problems with better efficiency and accuracy, since far-field representation is more rigorous than previously mentioned schemes. Another advantage is that the layered systems can be treated with a sound theoretical basis. The general coupling procedure of the boundary integral equation method with other numerical methods is discussed by Zienkiewicz *et al.* (1977) and Shaw (1978), and more recently by Wolf and Darbre (1984) and Chen and Penzien (1986) for dynamic soil structure interaction problems. A review of the literature reveals that the application of the coupled finite element–boundary integral scheme to elastostatic and elastodynamic problems involving semi-infinite media warrants further investigation. Conceptual aspects such as the occurrence of a non-symmetric stiffness matrix in the analysis and numerical aspects such as the selection of load and observation points in the boundary representation of exterior semi-infinite domain deserve particular attention. Furthermore, the application and verification of coupled schemes for elastodynamic problems involving layered systems have not been reported in the literature.

Present study

In this paper, consideration is given to the layered elastic half space system shown in Fig. 1 where a near-field region V' enclosing all inhomogeneities is modelled by conventional

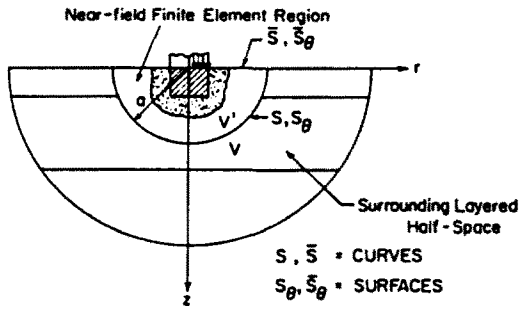

Fig. 1. Layered half space with inhomogeneities.

finite elements. The problems under consideration involve axisymmetric geometries and arbitrary loading.

The equation of motion of the near-field finite element region is developed through the application of Lagrange's equations of motion (Washizu, 1982) in classical elastodynamics. The incorporation of near-field finite elements to the variational formulation follows standard procedure. The influence of the far-field domain V on V' is modelled by separating V' from V along the contact surface S_θ and applying an appropriate contact traction field on S_θ. A linear relationship between displacement and traction vectors corresponding to nodes on the contact surface S_θ is developed through the consideration of the displacement Green's function for the exterior domain V. The Lagrangian function of the near-field domain which consists of volume integrals representing kinetic and strain energy of V' and a surface integral on S_θ representing the contribution due to the boundary traction field is expressed in terms of nodal displacement and velocity vectors. The substitution of the Lagrangian function in Lagrange's equations of motion and subsequent differentiation leads to the equations of motion of the near-field domain.

The present formulation guarantees a symmetric stiffness matrix for the entire system, regardless of the symmetry of the boundary traction–displacement relationship. This allows, as illustrated in this paper, the use of both direct and indirect versions of the boundary integral equation scheme in the analysis to develop the traction–displacement relationship along S_θ. The implementation of the present algorithm relies on the availability of displacement and traction Green's functions for the exterior domain. A brief discussion on relevant Green's functions is also presented.

In the numerical study, emphasis is placed on a comprehensive verification of the performance of the present algorithm when applied to solve elastostatic and elastodynamic problems rather than its application to a variety of complicated practical problems involving layered systems. The performance of the hybrid model is rigorously investigated for various parameters by studying the response due to a harmonic torsional patch load acting on the surface of a homogeneous half space. The applicability and the accuracy of the hybrid scheme is further confirmed by studying the response due to a harmonic vertical patch load acting on the free surface. The application of the hybrid scheme to layered systems is illustrated by studying torsional vibrations of a layered elastic half space under surface loading and comparisons are presented with the corresponding analytical solution. Next, the torsional vibration of a flexible cylinder embedded in a layered elastic half space is studied to illustrate the effectiveness of the present hybrid modelling.

HYBRID FORMULATION

In the proposed hybrid formulation, a near-field region V' enclosing all inhomogeneities is modelled using conventional finite elements. Without loss of generality, the geometry of the near-field region is selected as a hemispherical domain with radius a as shown in Fig. 1. At this stage, it is advantageous to nondimensionalize the entire problem including the coordinate frame with respect to a. The present class of problems is treated within the framework of the classical elastodynamic theory based on small displacements and infinitesimal strains. In what follows, a rigorous variational formulation which is based on Lagrange's equations of motion is presented to solve the system depicted in Fig. 1. Conventional Cartesian (x, y, z) and cylindrical (r, θ, z) coordinate systems are employed in the sequel.

In view of the axial symmetry of the geometry of the problem displacements, stresses and other relevant quantities may be expanded in a Fourier series with respect to the circumferential coordinate θ. For example, displacements $u_r(r, \theta, z, t)$, $u_\theta(r, \theta, z, t)$ and $u_z(r, \theta, z, t)$ in the r-, θ-, and z-directions, respectively, may be expressed as

$$u_r(r, \theta, z, t) = \sum_{n=0}^{\infty} [u_{rn}(r, z, t) \cos n\theta + \bar{u}_{rn}(r, z, t) \sin n\theta] \tag{1}$$

$$u_\theta(r, \theta, z, t) = \sum_{n=0}^{\infty} [u_{\theta n}(r, z, t) \sin n\theta - \bar{u}_{\theta n}(r, z, t) \cos n\theta] \tag{2}$$

$$u_z(r,\theta,z,t)=\sum_{n=0}^{\infty}[u_{zn}(r,z,t)\cos n\theta+\bar{u}_{zn}(r,z,t)\sin n\theta] \tag{3}$$

where u_{rn}, $u_{\theta n}$, u_{zn} denote symmetric components of displacements and $\bar{u}_{rn}$, $\bar{u}_{\theta n}$, $\bar{u}_{zn}$ denote antisymmetric components of displacement. The antisymmetric components appearing in the Fourier expansion may be suppressed without loss of generality and in what follows, only symmetric components are considered. The formulation for antisymmetric components may be obtained from that for the symmetric components by replacing cos $n\theta$ by sin $n\theta$ and sin $n\theta$ by $-\cos n\theta$. Furthermore, it is assumed that the motion under consideration is harmonic, which is characterized by the term $e^{i\omega t}$ (omitted in the sequel), where $i=\sqrt{-1}$.

Finite element domain

Consider the interior domain V' in Fig. 1, modelled using finite elements. The displacement vector $\mathbf{u}(r,\theta,z)$ and velocity vector $\dot{\mathbf{u}}(r,\theta,z)$ at a point within an element e having p nodes may be approximated by harmonics of the nodal displacement vector $\mathbf{q}_m^e$ and nodal velocity vector $\dot{\mathbf{q}}_m^e$

$$\mathbf{u}(r,\theta,z)=\sum_{m=0}^{\infty}[N][Q]_m\mathbf{q}_m^e \tag{4a}$$

$$\dot{\mathbf{u}}(r,\theta,z)=\sum_{m=0}^{\infty}[N][Q]_m\dot{\mathbf{q}}_m^e \tag{4b}$$

where

$$\mathbf{u}=\langle u_r \quad u_\theta \quad u_z\rangle^{\mathrm{T}};\quad \dot{\mathbf{u}}=\langle \dot{u}_r \quad \dot{u}_\theta \quad \dot{u}_z\rangle^{\mathrm{T}} \tag{5}$$

and $[N]$ is the displacement interpolation function matrix defined as

$$[N]=\begin{bmatrix}\mathbf{N} & \mathbf{0} & \mathbf{0}\\ \mathbf{0} & \mathbf{N} & \mathbf{0}\\ \mathbf{0} & \mathbf{0} & \mathbf{N}\end{bmatrix} \tag{6a}$$

with

$$\mathbf{N}=\langle N_1 \quad N_2 \quad \ldots \quad N_p\rangle^{\mathrm{T}} \tag{6b}$$

$$[Q]_m=\begin{bmatrix}[Q]_{1m} & & 0\\ & [Q]_{2m} & \\ 0 & & [Q]_{1m}\end{bmatrix} \tag{7a}$$

$$[Q]_{1m}=\cos m\theta[I];\quad [Q]_{2m}=\sin m\theta[I] \tag{7b}$$

$$\mathbf{q}_m^e=\langle \mathbf{q}_{rm}^e \quad \mathbf{q}_{\theta m}^e \quad \mathbf{q}_{zm}^e\rangle^{\mathrm{T}} \tag{8a}$$

$$\mathbf{q}_{\alpha m}^e=\langle u_{\alpha m}^1 \quad \ldots \quad u_{\alpha m}^p\rangle,\quad \alpha=r,\theta,z. \tag{8b}$$

In eqns (6), N_j ($j=1,\ldots,p$) denote nodal shape functions of a near-field isoparametric finite element, and the explicit representation of N_j is given by Zienkiewicz (1977). The symbol $[I]$ in eqns (7b) denotes a unit matrix. The mth harmonic of displacement in the α-direction of node j is denoted by $u_{\alpha m}^j$ ($\alpha=r,\theta,z$; $j=1,\ldots,p$). Also note that $\dot{\mathbf{q}}_m^e$ in eqn (4b) is defined similar to $\mathbf{q}_m^e$ in eqns (8).

The strain vector $\boldsymbol{\varepsilon}$ of an element can be expressed in terms of the harmonics of nodal displacement as

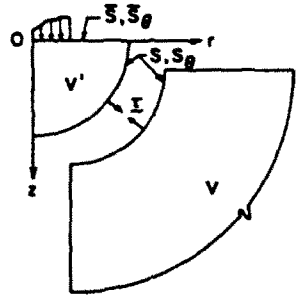

Fig. 2. Free-body diagrams of near- and far-field domains.

$$\varepsilon = \sum_{m=0}^{\infty} [B]_m q_m^e \tag{9}$$

where

$$\varepsilon = \langle \varepsilon_{rr} \quad \varepsilon_{zz} \quad \varepsilon_{\theta\theta} \quad \varepsilon_{rz} \quad \varepsilon_{r\theta} \quad \varepsilon_{\theta z} \rangle^T. \tag{10}$$

Note that the differential operator $[B]_m$ contains circumferential dependence. The relationship between the stress vector σ and the strain vector ε can be expressed as

$$\sigma = [D]\varepsilon. \tag{11}$$

where

$$\sigma = \langle \sigma_{rr} \quad \sigma_{zz} \quad \sigma_{\theta\theta} \quad \sigma_{rz} \quad \sigma_{r\theta} \quad \sigma_{\theta z} \rangle^T. \tag{12}$$

In eqn (11), $[D]$ is the constitutive matrix for the material (Fung, 1965).

Boundary surface

Consider the boundary surface S_0 which separates the interior finite element region V' and the exterior semi-infinite domain V as shown in Fig. 2. In view of the axial symmetry of the problem, S_0 is identical to the surface generated by the quarter-circle arc S in the r–z plane about the z-axis. Thus, a point $P(r, z)$ on S represents a circle with radius r. It is assumed that the boundary curve S has a total of n_b finite element nodes. The displacement vector $\mathbf{u}^b(r, \theta, z)$ and traction vector $\tau(r, \theta, z)$ at an arbitrary point on the boundary may be expressed as

$$\mathbf{u}^b(r, \theta, z) = \sum_{m=0}^{\infty} [N][Q]_m q_m^b \tag{13}$$

and

$$\tau(r, \theta, z) = \sum_{m=0}^{\infty} [N][Q]_m g_m. \tag{14}$$

In eqns (13) and (14), $[N]$ and $[Q]_m$ are defined similar to eqns (6) and (7), except that the size of these matrices is determined by the number of nodal points on S. In addition, g_m in eqn (14) denotes a vector consisting of m harmonic components of nodal tractions, and is defined as

$$g_m = \langle g_{rm} \quad g_{\theta m} \quad g_{zm} \rangle^T \tag{15a}$$

and

$$\mathbf{g}_{\alpha m} = \langle \tau_{\alpha m}^1 \quad \ldots \quad \tau_{\alpha m}^{n_b} \rangle, \quad \alpha = r, \theta, z. \tag{15b}$$

In eqns (15), $\tau_{\alpha m}^j$ denotes the mth harmonic of traction in the α-direction at node j ($j = 1, \ldots, n_b$).

Let $\bar{G}_{\alpha\beta}^m(r, z; s, z')\, f_\alpha^m(\theta)$, [$f_\alpha^m(\theta) = \cos m\theta$ for $\alpha = r, z$ and $f_\alpha^m(\theta) = \sin m\theta$ for $\alpha = \theta$] denote the displacement in the α-direction ($\alpha = r, \theta, z$) at point $P(r, \theta, z)$ in V due to a concentrated ring load in the β-direction ($\beta = r, \theta, z$) through the point $Q(s, z')$ on S. The circumferential distribution of the ring load is taken as $\cos m\theta$ for $\beta = r, z$ and $\sin m\theta$ for $\beta = \theta$. The following integral relationship can be established for a harmonic of displacement component within an arbitrary point in the r–z plane in V denoted by $u_{\alpha m}(r, z)$ as

$$u_{\alpha m}(r, z) = \int_S \bar{G}_{\alpha\beta}^m(r, z; s, z')\, \tau_{\beta m}(s, z')\, s\, \mathrm{d}S, \quad \alpha, \beta = r, \theta, z \quad (s, z') \in S. \tag{16}$$

In eqn (16), $\tau_{\beta m}$ denotes the mth harmonic of boundary traction component τ_β and summation is implied on index β. The vector $\boldsymbol{\tau}_m$ consisting of the mth harmonic components of traction at an arbitrary point on the boundary may be interpolated in terms of vector $\mathbf{g}_m$ consisting of the mth harmonic of tractions at boundary nodes as

$$\boldsymbol{\tau}_m(r, z) = [N]\mathbf{g}_m. \tag{17}$$

In view of eqns (13) and (17), the following relationship can be established by applying eqn (16) to nodal points:

$$\mathbf{q}_m^b = \int_S [\bar{G}_{\alpha\beta}]_m [N] \mathbf{g}_m s\, \mathrm{d}S \tag{18}$$

which may be expressed as

$$\mathbf{q}_m^b = [E]_m \mathbf{g}_m \tag{19}$$

where

$$[E]_m = \int_S [\bar{G}_{\alpha\beta}]_m [N]\, s\, \mathrm{d}S \tag{20}$$

or

$$\mathbf{g}_m = [G^*]_m \mathbf{q}_m^b \tag{21}$$

where $[G^*]_m = [E]_m^{-1}$

Equation (21) presents a linear relationship between nodal displacement and traction vectors for an arbitrary harmonic.

Substitution of eqn (21) in eqn (14) results in

$$\boldsymbol{\tau}(r, \theta, z) = \sum_{m=0}^{\infty} [N][Q]_m [G^*]_m \mathbf{q}_m^b. \tag{22}$$

Equation of motion of V'

Lagrange's equations of motion for the finite element domain are expressed as (Washizu, 1982)

$$\frac{\mathrm{d}}{\mathrm{d}t}\left(\frac{\partial L}{\partial \dot{\mathbf{q}}_m}\right)-\frac{\partial L}{\partial \mathbf{q}_m}=Q_m, \quad m=0,1,2\ldots \tag{23}$$

where the Lagrangian function of V'' denoted by L is defined as

$$L=\frac{1}{2}\int\int\int_{V''}(\rho\dot{\mathbf{u}}^{\mathrm{T}}\dot{\mathbf{u}}-\boldsymbol{\varepsilon}^{\mathrm{T}}\boldsymbol{\sigma})\,\mathrm{d}V''-\frac{1}{2}\int\int_{S_\theta}(\mathbf{u}^h)^{\mathrm{T}}\boldsymbol{\tau}\,\mathrm{d}S_\theta \tag{24}$$

and the generalized force vector Q_m is given by

$$Q_m=\int\int_{S_\theta}\mathbf{F}\frac{\partial \mathbf{u}^{\mathrm{T}}}{\partial \mathbf{q}_m}\mathrm{d}S_\theta. \tag{25}$$

In eqn (25), the vector $\mathbf{F}$ with components arranged in order similar to eqn (5) denotes the externally applied traction on surface S_θ of the finite element region. Note that terms associated with the volume integral in eqn (24) represents the kinetic and strain energy of domain V'', respectively. The surface integral over S_θ corresponds to the work done by the traction field on S_θ.

The substitution of eqns (4), (9), (11), (13), and (22) in eqn (24) results in an explicit representation for L in terms of nodal displacement and velocity vectors. These explicit representations are then substituted into eqn (23). Subsequent differentiations together with the orthogonality of trigonometric functions, and the assumption that motion is harmonic, leads to the following equations of motion for each harmonic m:

$$[-\omega^2[M]_m+[K]_m+[\bar{K}]_m]\mathbf{q}_m=\mathbf{P}_m, \quad m=0,1,2,\ldots \tag{26}$$

where

$$[M]_m=\sum_e\int\int\int_{V^e}\rho[Q]_m[N]^{\mathrm{T}}[N][Q]_m\,\mathrm{d}V^e \tag{27a}$$

$$[K]_m=\sum_e\int\int\int_{V^e}[B]_m^{\mathrm{t}}[D][B]_m\,\mathrm{d}V^e \tag{27b}$$

$$\mathbf{P}_m=\sum_e\int\int_{S_\theta^e}[Q]_m[N]^{\mathrm{T}}[N][Q]_m\mathbf{F}_m^e\,\mathrm{d}S_\theta^e \tag{27c}$$

$$\mathbf{q}_m=\sum_e\mathbf{q}_m^e. \tag{27d}$$

In the above equations, V^e denotes volume of a near-field element and S_θ^e denotes the surface area over which external tractions are applied on a near-field finite element. It can be observed that the first two terms in eqn (26) represent the standard form of symmetric mass and stiffness matrices of a near-field finite element region in an elastodynamic analysis. Note that circumferential dependence embedded in $[Q]_m$ in eqns (27) can be integrated analytically in the numerical implementation.

In eqn (26), $[\bar{K}_m]$ represents the contribution of the boundary tractions representing the influence of domain V on V'' to the equation of motion corresponding to the mth harmonic and defined as

$$[\bar{K}]_m=\begin{bmatrix}0 & 0\\ 0 & [H]_m\end{bmatrix}. \tag{28}$$

The square stiffness matrix $[H]_m$ of size $3n_h$ is defined as

$$[H]_m = \frac{1}{2}\int\int_{S_\theta} \{[G^*]_m^T[Q]_m[N]^T[N][Q]_m + [Q]_m[N]^T[N][Q]_m[G^*]_m\}\, dS_\theta. \quad (29)$$

It should be mentioned here that $[H]_m$ is symmetric irrespective of the symmetry of $[G^*]_m$ defining the relationship between the mth harmonic of nodal displacement and traction vectors at the boundary.

At this stage, attention is focused to studies by Wolf and Darbre (1984) and Chen and Penzien (1986), where the contribution of the exterior domain is incorporated into the equations of motion through the continuity of displacements and tractions at boundary nodal locations. In these formulations, $[G^*]_m$ enters into the analysis as a direct addition to the equation of motion. Therefore, the symmetry of the final equation system is violated unless $[G^*]_m$ is symmetric. As a consequence, a special technique such as the weighted-residual version of the indirect boundary element method has to be used to guarantee the symmetry of $[G^*]_m$. However, in the present formulation, the influence of exterior domain is incorporated directly into the variational treatment, instead of using a discrete continuity relationship. Consequently, the unconditional symmetry of $[H]_m$ allows the use of both direct and indirect versions of the boundary integral equation method without any special techniques.

THE BOUNDARY TRACTION–DISPLACEMENT RELATIONSHIP

The hybrid formulation presented in the preceding section relies on the existence of a traction–displacement relationship at boundary S. In eqn (16), such a relationship has been established between harmonics of displacement and traction at the boundary through the Green's function $\bar{G}^m_{\alpha\beta}(r, z; r', z')$ corresponding to domain V.

It is important to realize that the above Green's function is different from that corresponding to a uniform half space without a cavity. According to the authors' knowledge, a direct derivation of a Green's function for a half space with a cavity has not been reported in the literature, even for the simplest possible loading case. In the present study, the relationship between boundary traction and displacements is obtained through the application of integral representation theorems (Eringen and Suhubi, 1975) (direct boundary integral equation method) or the indirect boundary integral equation method due to Ohsaki (1973). These algorithms are based on displacement and traction Green's functions for a uniform (without a cavity) half space region.

Indirect method

First, consider the indirect boundary integral equation method due to Ohsaki (1973). The traction–displacement relationship at boundary S is developed by considering the uniform half space region. In this method, an arbitrary contour S' interior to S is selected as shown in Fig. 3. In a three-dimensional figure S and S' represent a hemispherical surface S_θ and S'_θ, respectively. Consider a force field τ' applied over the surface S'. In view of the axial symmetry, it is possible to develop the following relationships involving harmonics of displacements and tractions in S and harmonics of forces applied on S'

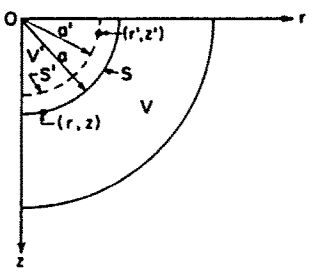

Fig. 3. Uniform half space region with contours S and S'.

$$u^h_{\alpha m}(r,z) = \int_{S'} G^m_{\alpha\beta}(r,z;r',z')\,\tau'_{\beta m}(r',z')r'\,\mathrm{d}S' \tag{30}$$

$$\tau_{\alpha m}(r,z) = \int_{S'} T^m_{\alpha\beta}(r,z;r',z')\,\tau'_{\beta m}(r',z')r'\,\mathrm{d}S', \quad (r,z)\in S, \quad (r',z')\in S'. \tag{31}$$

In eqns (30) and (31), $G^m_{\alpha\beta}(r,z;r',z')$ and $T^m_{\alpha\beta}(r,z;r',z')$ denote harmonics of displacements and traction in the α-direction at point (r,z) due to a ring load through point (r',z') in the β-direction. Note that $G^m_{\alpha\beta}$ and $T^m_{\alpha\beta}$ are displacement and traction Green's functions, respectively, for a uniform (undisturbed) half space. A discrete representation of eqn (30) may be obtained by considering a total of n'_t nodal points on S' and applying eqn (30) to n_h nodal locations on S. In doing so, the following representation is obtained:

$$\mathbf{q}^h_m = [A]_m \mathbf{g}'_m \tag{32}$$

where

$$[A]_m = \int_{S'} [G_{\alpha\beta}]_m [N] r'\,\mathrm{d}S'.$$

In eqn (32), $\mathbf{g}'_m$ is a vector containing the mth harmonic of forces applied on S' and it is defined similarly to $\mathbf{g}_m$ given by eqns (15). The number of nodal locations on S and S' need not be equal, since $\mathbf{g}'_m$ corresponding to a specified $\mathbf{q}^h_m$ may be obtained by solving eqn (32) in a least square sense. In doing so, the following relationship can be established:

$$\mathbf{g}'_m = [\bar{A}]_m \mathbf{q}^h_m \tag{33}$$

where

$$[\bar{A}]_m = [[A]^{\mathrm{T}}_m [A]_m]^{-1} [A]^{\mathrm{T}}_m.$$

The mth harmonic of the force vector τ'_m at a point may be interpolated in terms of nodal vector $\mathbf{g}'_m$ as

$$\tau'_m = [N]\mathbf{g}'_m. \tag{34}$$

Substitution of eqns (33) and (34) into eqns (31) yields

$$\tau_{\alpha m}(r,z) = \int_{S'} \langle T^m \rangle [N][\bar{A}]_m \mathbf{q}^h_m r'\,\mathrm{d}S' \tag{35}$$

where

$$\langle T^m \rangle = \langle \mathbf{T}^m_{zr} \quad \mathbf{T}^m_{z\theta} \quad \mathbf{T}^m_{zz} \rangle, \quad (r,z)\in S$$

$$\mathbf{T}^m_{\alpha\beta} = \langle T^m_{\alpha\beta}(r,z;r',z') \rangle_{1\times n'_t}.$$

The application of eqn (35) to nodal locations on S leads to the following relationship between the mth harmonic of the nodal traction vector $\mathbf{g}_m$ and the displacement vector $\mathbf{q}^h_m$:

$$\mathbf{g}_m = \left\{ \int_{S'} [T^m_{z\beta}][N][\bar{A}]_m r' \, dS' \right\} \mathbf{q}^h_m. \tag{36a}$$

Comparison of eqns (21) and (36a) implies that

$$[G^*]_m = \int_{S'} [T^m_{z\beta}][N][\bar{A}]_m r' \, dS'. \tag{36b}$$

Direct method

As an alternative to the above indirect boundary integral equation algorithm, one can also use the integral representation theorem for an elastic solid (Eringen and Suhubi, 1975) to obtain a representation for $[G^*]$ in terms of tractions and displacement Green's functions for a uniform half space. In the case of systems involving axial symmetry, a reduced version of representation theorems may be written as

$$\delta(r', z') u_{zm}(r', z') = \int_S [G^m_{\beta z}(r, z; r', z') \tau_{\beta m}(r, z) - T^m_{\beta z}(r, z; r', z') u^h_{\beta m}(r, z)] \, r \, dS \tag{37}$$

where

$$\delta(r', z') = \begin{cases} 0, & (r', z') \in V' \\ \frac{1}{2}, & (r', z') \in S \\ 1, & (r', z') \in V. \end{cases} \tag{38}$$

The application of eqn (37) with $(r', z') \in V'$ leads to the identity

$$\int_S G^m_{\beta z}(r, z; r', z') \tau_{\beta m}(r, z) r \, dS = \int_S T^m_{\beta z}(r, z; r', z') u^h_{\beta m}(r, z) r \, dS, \quad (r', z') \in V', (r, z) \in S. \tag{39}$$

Note that $\tau_{\beta m}(r, z)$ and $u^h_{\beta m}(r, z)$ of boundary S may be interpolated in terms of nodal vectors $\mathbf{g}_m$ and $\mathbf{q}^h_m$, respectively, as given by eqns (14) and (13). This, together with the consideration of a set of points on an arbitrary contour S' (Fig. 3) yields a discrete version of eqn (39) as

$$[B]_m \mathbf{g}_m = [C]_m \mathbf{q}^h_m \tag{40}$$

where

$$[B]_m = \int_S [G_{\beta z}]^m [N] r \, dS \tag{41}$$

and

$$[C]_m = \int_S [T_{z\beta}]^m [N] r \, dS. \tag{42}$$

A direct representation of $\mathbf{g}_m$ in terms of $\mathbf{q}^h_m$ may be obtained from eqn (40) if the number of points selected on S and S' are equal. In this case

$$\mathbf{g}_m = [B]_m^{-1}[C]_m \mathbf{q}_m^b. \tag{43}$$

The above equation implies that $[G^*]_m$ in eqn (21) may be expressed as

$$[G^*]_m = [B]_m^{-1}[C]_m. \tag{44}$$

Comparison of eqns (36b) and (44) shows that in both methods load sources are considered on S'. In the direct method, ring load sources acting at discrete points on S' are used whereas in the indirect method loading sources distributed along the entire contour S' are used. On the other hand, in the direct method the entire contour S is incorporated into the analysis, whereas in the indirect method only discrete points located on S are used. When the number of nodal points considered on S and S' are equal, the indirect method reduces to a representation similar to that obtained from the direct method. However, the associated matrices involve integrals defined over two different contours.

Another representation for $\mathbf{g}_m$ derived on the basis of eqn (37) for a given $\mathbf{q}_m^b$ which does not require that the number of nodal points on S and S' be equal is presented by Apsel (1979). Apsel's scheme leads to a representation similar in structure to that obtained through the application of Ohsaki's scheme (1973) as given by eqn (36b).

At this stage, it can be stated that the boundary traction–displacement relationship $[G^*]_m$ for a given harmonic can be established by using eqn (36b) or eqn (44). Any of these representations of $[G^*]_m$ will allow the computation of $[H]_m$ in eqn (29). Thereafter, eqn (26) is solved for $\mathbf{q}_m$ corresponding to a given geometric and loading configuration. Representations for $[G^*]_m$ involve matrices the elements of which are displacement and traction Green's functions for a half space due to ring loads with circumferential dependence $f_\tau^m(\theta)$. A brief discussion on the derivation of these Green's functions is presented in the following section.

Green's functions

The establishment of traction–displacement relationship $[G^*]_m$ relies on the availability of Green's functions corresponding to a uniform half space in the absence of any inhomogeneity. The general solution to equations of equilibrium for a three-dimensional elastic solid may be obtained through the application of Hankel integral transform techniques. The study by Harding and Sneddon (1945) presents perhaps the earliest application of Hankel integral transforms in the solution of boundary-value problems in classical elasticity. A later study by Muki (1960) presented a generalization of the solution approach of Harding and Sneddon (1945) to solve boundary-value problems in elastostatics involving axisymmetric geometries under arbitrary loading. Later studies by Westmann (1964) and Chan *et al.* (1974) demonstrated the application of Muki's approach to obtain elastostatic Green's functions for layered media. A general formulation for elastostatics of layered systems in terms of Fourier integrals has been presented by Chen (1971). The dynamic response of a multi-layered half space has been investigated by many researchers over the past several years. Among others, Thompson (1950), Haskell (1953), Jardetzky (1953), Harkrider (1964, 1970), Schwab (1970), Apsel (1979), Luco and Apsel (1983) and Apsel and Luco (1983) studied various aspects of the dynamic Green's functions of a multi-layered half space.

These studies indicate that in general, the explicit derivation of Green's functions $G_{z\beta}^m$ and $T_{z\beta}^m$ for an arbitrary harmonic m is possible only in the case of a homogeneous half space. The tedious nature of algebra involved in the derivation of Green's functions for layered systems can be seen from the solution of Chan *et al.* (1974), where a static loading at the interior of a single-layered half space system is considered. In the case of multi-layered systems, the most efficient way is to solve numerically for arbitrary functions appearing in the general solution and to construct all Green's functions through an appropriate numerical integration scheme. The studies of Apsel (1979), Luco and Apsel (1983) and Apsel and Luco (1983) present a concise treatment of the evaluation of Green's functions for a multi-layered elastic half space. A systematic procedure for the numerical evaluation of Green's functions, its implementation and various computational aspects are discussed in detail in these references.

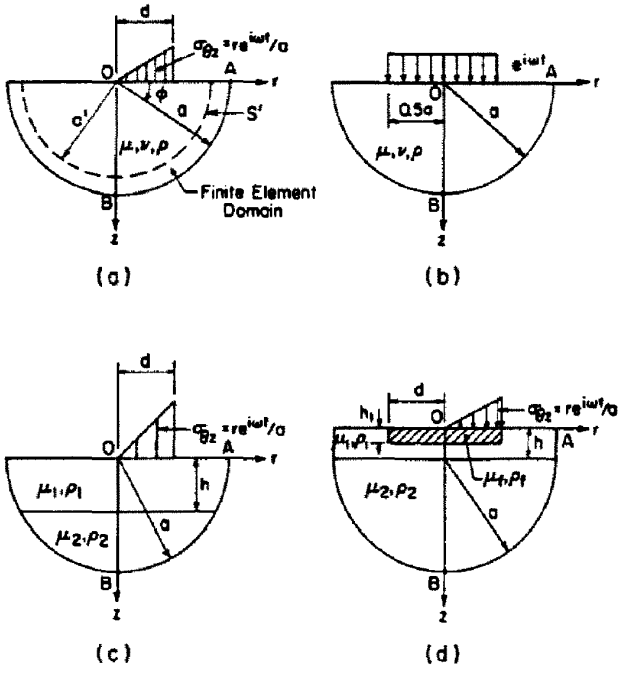

Fig. 4. Geometries and loading configurations: (a) torsional load on homogeneous half space; (b) uniform vertical pressure on homogeneous half space; (c) torsional load on layered half space; (d) torsionally load embedded cylinder in layered half space.

NUMERICAL RESULTS

In the numerical study, the performance of the present hybrid algorithm is investigated by considering a few boundary-value problems associated with semi-infinite media for which analytical solutions can be derived.

Problem 1

The problem of a homogeneous elastic half space subjected to a linearly varying static ($\omega = 0$) torsional patch load applied over a circular area at the surface level, as shown in Fig. 4(a) is considered. The analytical solution corresponding to this boundary value problem may be obtained from the fundamental solutions presented by Karasudhi *et al.* (1984). Their solution is expressed in terms of infinite integrals of the Lipschitz–Hankel type, which may be expressed in terms of elliptic integrals by using identities given by Eason *et al.* (1955). At present, mathematical software is available to compute elliptic integrals with very high numerical precision. Therefore, the elastostatic solution corresponding to the loading configuration shown in Fig. 4(a) can be computed very accurately without adopting computationally expensive and less accurate numerical integration schemes. The near-field finite element meshes (eight-node elements) used in the hybrid scheme are shown in Figs 5(a)–(c). These represent relatively coarse to finer mesh configurations. Note that for the loading configuration shown in Fig. 4(a), u_r and u_z are identically zero. Displacement and traction Green's functions required in the computation of $[G^*]_0$ of the exterior domain have been given (Rajapakse and Selvadurai, 1985). The resulting expressions consisting of infinite integrals are then expressed in terms of elliptic integrals (Eason *et al.*, 1955) for numerical evaluation.

At this stage, it is useful to define a measure of the error of displacement for the purpose of comparison. The Euclidean norm of the error of displacement in the θ-direction along a specified contour is defined as

$$E_k = \left[\left(\sum_{j=1}^{n_k} \bar{u}_{\theta j}^2\right)^{1/2} - \left(\sum_{j=1}^{n_k} u_{\theta j}^2\right)^{1/2}\right] \Big/ \left(\sum_{j=1}^{n_k} \bar{u}_{\theta j}^2\right)^{1/2}, \quad k = b, \bar{s}. \tag{45}$$

In eqn (45), subscripts b and $\bar{s}$ are used to denote quantities associated with the finite

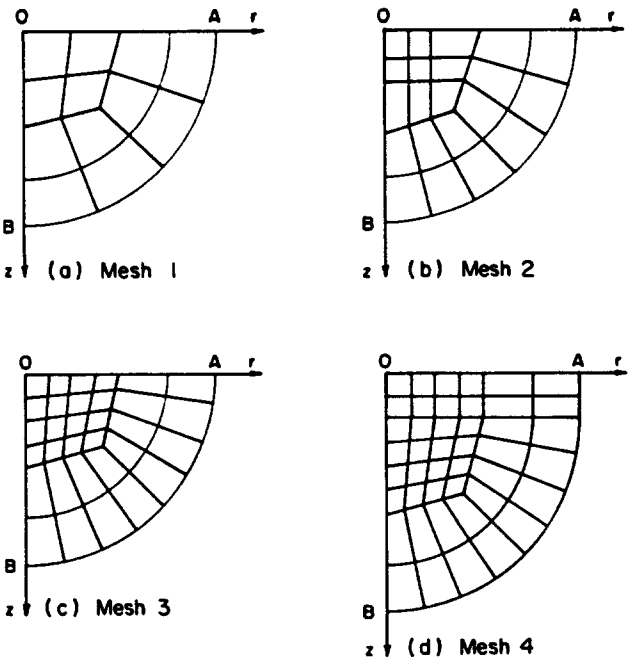

Fig. 5. Near-field finite element meshes.

Table 1. Comparison of Euclidean norm of error of displacement u_θ for various mesh configurations shown in Fig. 5 and location of S' for static loading shown in Fig. 4(a): $\mu = 1$, $d/a = 0.5$

Mesh number	E_t (%)				E_h (%)			
	$\bar{b} = 0.95$	$\bar{b} = 0.9$	$\bar{b} = 0.85$	$\bar{b} = 0.75$	$\bar{b} = 0.95$	$\bar{b} = 0.9$	$\bar{b} = 0.85$	$\bar{b} = 0.75$
Mesh 1	−2.41	−1.21	−0.988	−0.940	−20.12	−3.66	−0.505	0.110
Mesh 2	−0.67	−0.154	−0.111	−0.108	−8.97	−0.700	−0.040	−0.009
Mesh 3	−0.426	−0.193	−0.179	−0.174	−0.428	−0.378	−0.233	−0.225

element boundary (BA) and surface level (OA); n_h and n_t denote the number of nodal locations on BA and OA, respectively; $u_{\theta j}$ denotes displacement in the θ-direction at node j obtained from the hybrid scheme and $\tilde{u}_{\theta j}$ denotes the corresponding analytical solution.

Table 1 presents numerical values for E_h and E_t obtained from the present hybrid scheme for three finite element meshes shown in Fig. 5. These results correspond to four different locations of contour S' characterized by $\bar{b}$ $(=a'/a)$ and $[G^*]_0$ obtained using eqn (44), which is based on a direct application of integral representation theorems. In most cases, the tabulated error norms are very small, indicating the high accuracy of the present hybrid scheme. It can be seen that for $\bar{b} = 0.95$, the value of E_h is quite large when compared to E_h for other values of $\bar{b}$. This is due to the fact that as $\bar{b} \to 1$, Green's functions approach singular values, resulting in ill-conditioned matrices in the process of evaluation of $[G^*]_0$. In general, the results presented in Table 1 suggest that near exact solutions can be obtained from the present hybrid algorithm using any of the finite element meshes shown in Fig. 5 with $0.75 \leqslant \bar{b} \leqslant 0.90$. Table 2 presents numerical values of E_t and E_h when Ohsaki's scheme (eqn (36b)) is used to compute $[G^*]_0$. These results correspond to two locations of contour

Table 2. Comparison of Euclidean norm of error of displacement u_θ for static torsional loading shown in Fig. 4(a) with $[G^*]_0$ computed using equation (36b): $\mu = 1$, $d/a = 0.5$

Number of sources	E_t (%)		E_h (%)	
	$\bar{b} = 0.90$	$\bar{b} = 0.85$	$\bar{b} = 0.90$	$\bar{b} = 0.85$
6	−0.065	−0.132	1.18	0.305
8	0.148	−0.152	0.126	0.084
10	−0.160	−0.155	−0.041	0.026

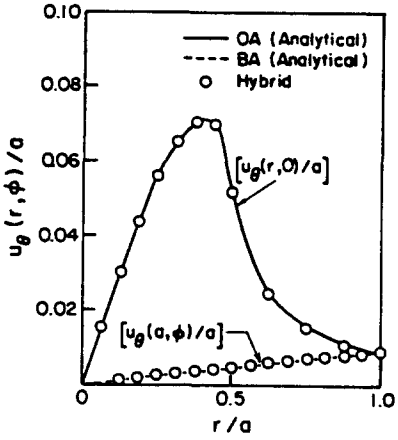

Fig. 6. Comparison of displacement profiles for static torsional loading ($\mu = 1$, $\rho = 1$, $d/a = 0.5$).

S' defined by $\bar{b} = 0.9$, 0.85 and three different values for the total number of divisions n_s' on S'. For brevity only the numerical results corresponding to the finite element mesh shown in Fig. 5(b) are presented. A comparison of non-dimensionalized displacement profiles along OA and BA obtained from the hybrid model with the corresponding analytical solutions are presented in Fig. 6. The high accuracy of the hybrid model is confirmed by results presented in Tables 1 and 2 and Fig. 6, irrespective of the scheme employed to obtain $[G^*]_0$. Solutions presented in the remainder of this paper are based on $[G^*]_m$ computed using eqn (36b).

Problem 2

Attention is next focused on the elastodynamic torsional loading problem shown in Fig. 4(a). The relevant non-dimensionalized frequency parameter a_0 is defined as $a_0 = ak_s$, where k_s is the shear wave number (Achenbach, 1973) corresponding to the surrounding half space. The analytical solution corresponding to this loading configuration may be obtained through the application of Hankel integral transforms. The relevant Green's functions required to compute $[G^*]_0$ have been presented (Rajapakse *et al.*, 1987). Unlike in the elastostatic case, all infinite integrals associated with analytical solutions for the loading configuration shown in Fig. 4(a) and those involved with the computation of $[G^*]_0$ have to be evaluated using a numerical integration scheme. In this study, the standard Simpson's rule with a sufficiently small interval of integration is used. In general, special attention is required in the evaluation of these complex-valued infinite integrals, since the integrand is of an oscillatory nature, and decays very slowly when $z \to z'$ (Fig. 3). For elastodynamic problems, $\mathbf{q}_m$ resulting from the solution of eqn (26), is complex. The error norms are computed separately using eqn (45) for both real and imaginary parts of solutions.

Table 3 presents E_r and E_h along OA and BA, respectively, for $a_0 = 1.25$ and 2.0. The source contour S' is located at $\bar{b} = 0.9$ and discretization configurations represented by $n_s' = 8$–14 are considered for S'. The finite element mesh shown in Fig. 5(c) is selected to satisfy requirements on the size of a finite element in elastodynamic analysis (Medina and Penzien, 1982; Rajapakse and Karasudhi, 1986). The low values of E_r and E_h in Table 3 indicate the accuracy of the hybrid model for elastodynamic problems. Error norms for the

Table 3. Comparisons of error norms along the boundary and surface for time-harmonic torsional loading system shown in Fig. 4(a): $\rho = 1$, $\mu = 1$, $\bar{b} = 0.9$, $n_h = 16$

	$a_0 = 1.25$		$a_0 = 2.00$	
n_s'	E_r (%)	E_h (%)	E_r (%)	E_h (%)
8	(0.39, 7.14)	(5.36, 3.65)	(0.09, 6.76)	(5.57, 4.23)
10	(0.20, 1.75)	(3.14, 0.26)	(0.06, 3.02)	(4.94, 1.91)
12	(−0.09, 3.50)	(−1.32, −7.37)	(0.01, −1.02)	(4.14, −4.69)
14	(0.09, 1.07)	(1.25, −1.62)	(−0.08, 2.36)	(3.34, −0.05)

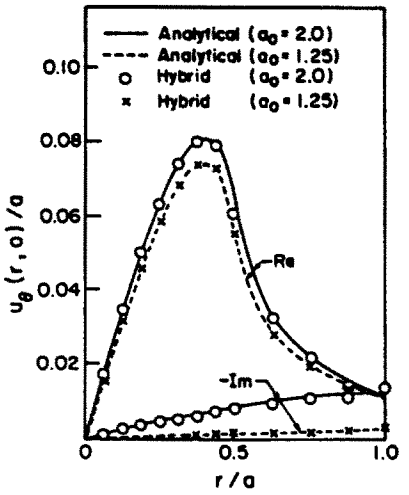

Fig. 7. Comparison of surface displacement profiles for harmonic torsional loading ($\mu = 1$, $\rho = 1$, $d/a = 0.5$).

imaginary part of displacement are found to be slightly higher than those of real parts. In general, the error norm along the boundary (E_h) is higher than those for the static problem. Figure 7 presents a comparison of the non-dimensionalized surface displacement profile along OA for $a_0 = 1.25$ and 2.0. The corresponding displacement profiles along the finite element boundary BA are presented in Fig. 8. The high accuracy of the present hybrid model is confirmed by these results for elastodynamic problems.

Problem 3

The next problem considered is that corresponding to a uniform harmonic vertical pressure applied over a circular area on the surface as shown in Fig. 4(b). The analytical solution corresponding to this loading configuration has been given for elastostatic and elastodynamic cases (Selvadurai and Rajapakse, 1985; Rajapakse and Shah, 1987). For

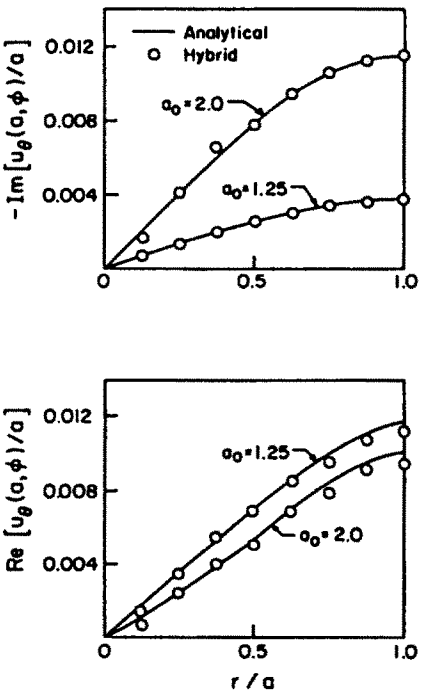

Fig. 8. Comparison of boundary displacement profiles for harmonic torsional loading ($\mu = 1$, $\rho = 1$, $d/a = 0.5$).

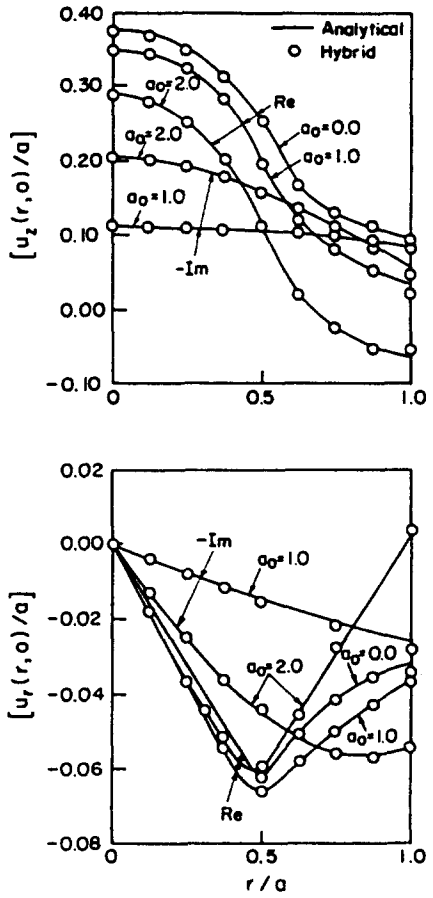

Fig. 9. Comparison of surface displacement profiles under uniform unit harmonic vertical pressure ($\mu = 1$, $\rho = 1$, $\nu = 0.25$, $\beta = 0.85$, $n_s' = 8$).

the static problem, the analytical solution and Green's functions required in the evaluation of $[G^*]_m$ are computed by expressing all infinite integrals in terms of elliptic integrals. For elastodynamic problems, the integrands of infinite integrals associated with the analytical solution and Green's functions are singular at k_s, k_p and k_r, where k_s, k_p and k_r denote wave numbers of shear, compressional and Rayleigh waves (Achenbach, 1973) of the surrounding half space. All Green's functions required in the computation of $[G^*]_0$ corresponding to the elastodynamic problem are evaluated using numerical integration along an appropriate contour in the first quadrant of the complex plane (Rajapakse and Shah, 1987). A comparison of surface displacement profiles for both u_z and u_r obtained using a finite element mesh shown in Fig. 5(c) are presented in Fig. 9. These results confirm the applicability and accuracy of the present hybrid model under general loading configurations, and a wide range of frequencies of applied loading.

Problem 4

The next problem considered in the numerical study is the case of torsional vibrations of a *layered* elastic half space under the surface loading configuration shown in Fig. 4(c). The finite element mesh of Fig. 5(d) is used. The analytical solution and Green's functions required to compute $[G^*]_0$ corresponding to this problem are derived by using Hankel integral transforms. A comparison of surface displacement profiles over a wide range of frequency of excitation is presented in Fig. 10. Note that in this problem, $a_0 = ak_s'$, where k_s' is the shear wave number of the layer. The accuracy of the hybrid model for elastodynamic problems involving layered systems is confirmed by solutions presented in Fig. 10. Solutions

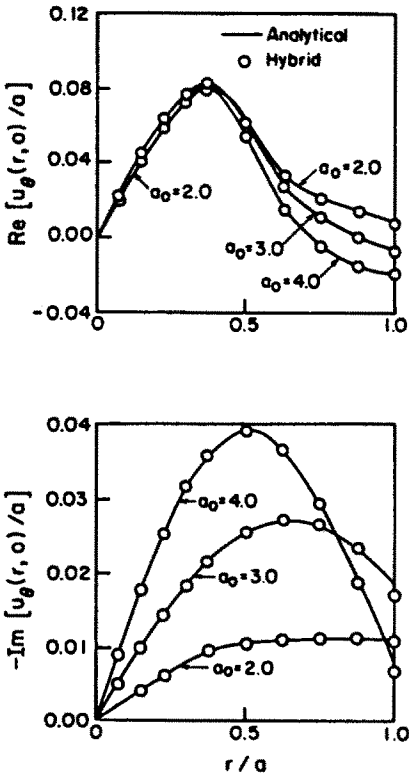

Fig. 10. Comparison of surface displacement profiles of the layered half space under harmonic torsional loading ($\mu_1 = 2\mu_2 = 1$, $\rho_1 = \rho_2 = 1$, $h/a = 0.5$, $d/a = 0.5$, $\bar{b} = 0.85$, $n_r' = 10$, $n_h = 21$).

were also obtained by varying $\bar{b}$ from 0.90 to 0.75 and n_r' from 12 to 8 and these variations showed negligible influence on the solution.

Figure 11 shows surface displacement profiles obtained from the present study for a layered half space containing a flexible cylindrical inclusion, as shown in Fig. 4(d), under a harmonic torsional loading applied at the surface level. The results were obtained employing the mesh of Fig. 5(d). It is noted that the flexibility of the cylinder has a significant influence on the real part of the displacement within $r/a = 0.6$, and its influence on the imaginary component is negligible. A similar behaviour of the imaginary component was observed (Rajapakse *et al.*, 1987) where an approximate analysis is presented for a flexible hemispherical foundation embedded in a homogeneous half space.

DISCUSSION AND CONCLUSIONS

The accuracy and efficiency of the present hybrid model is confirmed by the above numerical examples. The extension to elastostatic or elastodynamic problems involving a multi-layered half space does not involve any complications except the implementation of a more generalized sub-program for the numerical evaluation of Green's functions. Since conventional finite elements are used to model near field a variety of axisymmetric geometries and material properties may be considered for near-field inhomogeneities. It should also be mentioned here that the present method does not impose any restriction on the geometry of contours S and S', although in this study these are selected as quarter-circles for homogeneous half space problems. In the case of layered media (Rajapakse and Karasudhi, 1985), it is convenient to take contours S and S' parallel to the z-axis within the layers and as quarter-circles in the underlying half space, respectively, as shown in Fig. 5(d). The extension of the hybrid model to plane and general three-dimensional problems involves only the substitution of relevant basic equations for displacements, strains, and stresses.

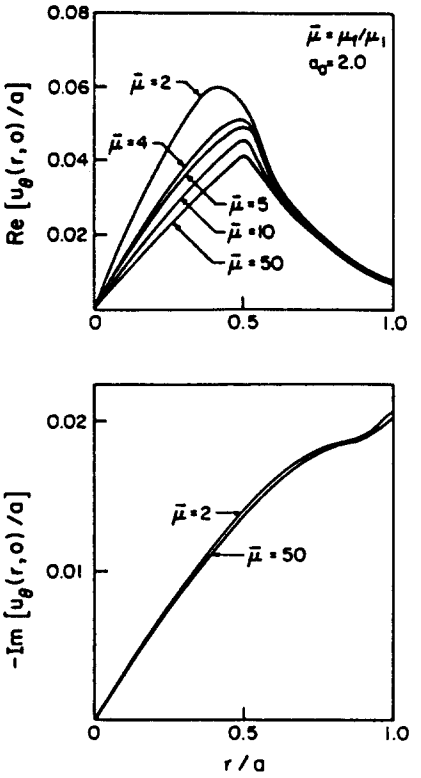

Fig. 11. Surface displacement profiles for a layered half space containing a torsionally loaded elastic cylinder ($\mu_1 = 2\mu_2 = 1$, $\rho_1 = \rho_2 = \rho_f = 1$, $h/a = 0.4$, $h_1/a = 0.25$, $d/a = 0.5$, $\bar{b} = 0.85$, $n_r' = 10$, $n_h = 21$).

Based on the comprehensive study presented in this paper, the following conclusions are drawn.

(a) The hybrid formulation presented in this study provides an accurate and efficient solution procedure for elastostatic and elastodynamic problems involving layered semi-infinite media.

(b) The present formulation guarantees a symmetric stiffness matrix in the analysis. This allows the use of both direct and indirect versions of the boundary integral equation method in the analysis.

(c) It is desirable from a computational point of view to select the contour S' sufficiently away from the finite element boundary and to use widely spaced source points on S' to avoid ill-conditioned matrices in the process of evaluation of $[G^*]_m$. In view of this, it is recommended that eqn (36b) is used to compute $[G^*]_m$ instead of eqn (44). This enhances the computational efficiency and numerical stability of the present algorithm. Alternatively, $[G^*]_m$ can be obtained from the direct boundary integral equation by using the scheme proposed by Apsel (1979).

Acknowledgement—The work presented here was supported by grants A-6507 and A-7988 from the Natural Science and Engineering Research Council of Canada. The authors are greatly indebted to the reviewers of this paper for their meticulous review and suggested revisions.

REFERENCES

Achenbach, J. D. (1973). *Wave Propagation in Elastic Solids*. North-Holland, Amsterdam.

Anderson, D. L. and Ungless, R. F. (1977). Infinite finite elements. *Proc. Int. Symp. on Innovative Numerical Analysis in Applied Engineering Sciences*, Paris, France.

Apsel, R. J. (1979). Dynamic Green's functions for layered media and applications to boundary-value problems. Ph.D. Thesis, University of California, San Diego, California.

Apsel, R. J. and Luco, L. E. (1983). On the Green's functions for a layered half-space, Part II. *Bull. Seism. Soc. Am.* 73, 931–951.

Avanessian, V., Dong, S. B. and Muki, R. (1986a). Axisymmetric soil–structure interaction by global–local finite elements. *Earthquake Engng Struct. Dyn.* 14, 355–367.

Avanessian, V., Muki, R. and Dong, S. B. (1986b). Forced oscillation of an axisymmetric structure in contact with an elastic half-space by a version of global–local finite elements. *J. Sound Vibr.* **104**, 449–463.
Bettes, P. (1977). Infinite elements. *Int. J. Numer. Meth. Engng* **11**, 53–64.
Bettes, P. and Zienkiewicz, O. C. (1977). Diffraction and refraction of surface waves using finite and infinite elements. *Int. J. Numer. Meth. Engng* **11**, 1271–1290.
Boussinesq, J. (1885). *Applications des Potentiels a l'Etude de l'Equilibre et du Mouvement des Solides Elastiques*. Gauthier-Villars, Paris, France.
Cerruti, V. (1882). *Acc. Lincei. Mem. Fis. Mat., Roma* **3**, 81.
Chan, K. S., Karasudhi, P. and Lee, S. L. (1974). Force at a point in the interior of a layered elastic halfspace. *Int. J. Solids Structures* **10**, 1179–1199.
Chen, W. T. (1971). Computation of stresses and displacements in layered media. *Int. J. Engng Sci.* **9**, 775–800.
Chen, C. and Penzien, J. (1986). Dynamic modelling of axisymmetric foundations. *Earthquake Engng Struct. Dyn.* **14**, 823–840.
Chow, Y. K. and Smith, I. M. (1981). Static and periodic infinite solid elements. *Int. J. Numer. Meth. Engng* **17**, 503–526.
Cruse, T. A. (1968). A direct formulation and numerical solution of the general transient elastodynamic problem II. *J. Math. Analysis Applic.* **21**, 341–355.
Cruse, T. A. and Rizzo, F. J. (1968). A direct formulation and numerical solution of the general transient elastodynamic problem I. *J. Math. Analysis Applic.* **22**, 244–259.
Cruse, T. A. and Rizzo, F. J. (Editors) (1975). *Boundary Integral Equation Method: Computational Applications in Applied Mechanics*, ASME, AMD-Vol. 11.
Cruse, T. A., Pifko, A. B. and Armen, H. (Editors) (1985). *Advanced Topics in Boundary Element Analysis*, ASME, AMD-Vol. 72.
Dong, S. B. (1981). Global–local finite element methods. In *State-of-the-Art Survey of Finite Element Methods* (Edited by W. D. Pilkey and A. K. Noor), Chap. 14. ASME.
Eason, E., Noble, B. and Sneddon, I. N. (1955). On certain integrals of Lipschitz–Hankel type involving products of Bessel functions. *Phil. Trans. R. Soc. London* **247**, 529–551.
Eringen, A. C. and Suhubi, E. (1975). *Elastodynamics*, Vol. II. Academic Press, New York.
Fung, Y. C. (1965). *Foundations of Solid Mechanics*. Prentice-Hall, Englewood Cliffs, New Jersey.
Goetschel, D. B., Dong, S. B. and Muki, R. (1982). A global–local finite element analysis of axisymmetric scattering of elastic waves. *J. Appl. Mech. ASME* **49**, 816–820.
Harding, J. W. and Sneddon, I. N. (1945). The elastic stresses produced by the indentation of the plane surface of a semi-infinite elastic solid by a rigid punch. *Proc. Camb. Phil. Soc.* **41**, 16–26.
Harkrider, D. G. (1964). Surface waves in multilayered elastic media, Part I—Rayleigh and Love waves from buried sources in a multilayered elastic half-space. *Bull. Seism. Soc. Am.* **54**, 627–680.
Harkrider, D. G. (1970). Surface waves in multilayered elastic media, Part II—Higher mode spectra and spectral ratios from point sources in plane layered earth models. *Bull. Seism. Soc. Am.* **60**, 1937–1987.
Haskell, N. A. (1953). The dispersion of surface waves in multilayered media. *Bull. Seism. Soc. Am.* **43**, 17–34.
Jardetzky, W. (1953). Period equation for a *n*-layered half space and some related questions. Technical Report, Seismology 29, Lamong Geological Observatory, Columbia University.
Karasudhi, P., Rajapakse, R. K. N. D. and Hwang, B. Y. (1984). Torsion of a long cylindrical bar partially embedded in a layered elastic half space. *Int. J. Solids Structures* **20**, 1–11.
Kausel, E., Roesett, J. M. and Wass, G. (1975). Dynamic analysis of footing on layered media. *J. Engng Mech. ASCE* **101**, 679–693.
Kobayashi, S. (1984). Fundamentals of boundary integral equation methods in elastodynamics. In *Topics in Boundary Element Research* (Edited by C. A. Brebbia), Chap. 1, pp. 1–54. Springer, Berlin.
Lamb, H. (1904). On the propagation of tremors over the surface of an elastic solid. *Phil. Trans. R. Soc. London* **A203**, 1–42.
Luco, J. E. and Apsel, R. J. (1983). On the Green's functions for a layered half-space, Part I. *Bull. Seism. Soc. Am.* **73**, 909–929.
Lysmer, J. and Kuhlemeyer, R. L. (1969). Finite dynamic model for infinite media. *J. Engng Mech. Div. ASCE* **95**, 859–877.
Medina, F. and Penzien, J. (1982). Infinite elements for elastodynamics. *Earthquake Engng Struct. Dyn.* **10**, 699–709.
Mindlin, R. D. (1936). Force at a point in the interior of a semi-infinite solid. *Physics* **7**, 195–202.
Mote, G. D. (1971). Global–local finite element. *Int. J. Numer. Meth. Engng* **3**, 565–574.
Muki, R. (1960). Asymmetric problems of the theory of elasticity for a semi-infinite solid and a thick plate. In *Progress in Solid Mechanics* (Edited by I. N. Sneddon and R. Hill), Vol. I. North-Holland, Amsterdam/Interscience, New York.
Muki, R. and Dong, S. B. (1979). Some remarks on the use of asymptotic solutions in global–local finite element analysis for an elastic half space. In *Recent Research on Mechanical Behaviour of Solids*, pp. 55–78. University of Tokyo Press, Tokyo.
Muki, R. and Dong, S. B. (1980). Elastostatic far field behaviour in a layered half space under surface pressure. *J. Appl. Mech. ASME* **47**, 504–512.
Ohsaki, Y. (1973). On movement of a rigid body in semi-infinite elastic medium. *Proc. Japan Earthquake Engng Symp.*, Tokyo, Japan, pp. 245–252.
Rajapakse, R. K. N. D. and Karasudhi, P. (1985). Elastostatic infinite elements for layered half spaces. *J. Engng Mech. ASCE* **111**, 1144–1158.
Rajapakse, R. K. N. D. and Karasudhi, P. (1986). An efficient elastodynamic infinite element. *Int. J. Solids Structures* **22**, 643–657.
Rajapakse, R. K. N. D. and Selvadurai, A. P. S. (1985). Torsional stiffness of non-uniform and hollow rigid piers embedded in isotropic elastic media. *Int. J. Numer. Analytical Meth. Geomech.* **9**, 525–539.
Rajapakse, R. K. N. D. and Shah, A. H. (1987). On the longitudinal harmonic motion of an elastic bar embedded in an elastic half space. *Int. J. Solids Structures* **23**, 287–303.

Rajapakse, R. K. N. D., Shah, A. H. and Datta, S. K. (1987). Torsional vibrations of elastic foundations embedded in elastic half-space. *Earthquake Engng Struct. Dyn.* **15**, 279–297.

Rizzo, R. J. (1967). An integral equation approach to boundary value problems of classical elastostatics. *Q. Appl. Math.* **25**, 84–95.

Rizzo, F. J., Shippy, D. J. and Rezayat, M. (1985). A boundary integral equation method for radiation and scattering of elastic waves in three dimensions. *Int. J. Numer. Meth. Engng* **21**, 115–129.

Schwab, F. (1970). Surface-wave dispersion computations: Knopoff's method. *Bull. Seism. Soc. Am.* **60**, 1491–1520.

Selvadurai, A. P. S. and Rajapakse, R. K. N. D. (1985). On the load transfer from a rigid cylindrical inclusion into an elastic half space. *Int. J. Solids Structures* **21**, 1213–1229.

Shaw, R. P. (1978). Coupling boundary integral equation method to other numerical techniques. In *Recent Advances in Boundary Element Methods* (Edited by C. A. Brebbia), pp. 137–147. Pentech Press, London.

Thompson, W. T. (1950). Transmission of elastic waves through a stratified solid medium. *J. Appl. Phys.* **21**, 89–93.

Waas, G. (1972). Linear two-dimensional analysis of soil dynamics problems in semi-infinite layered media. Ph.D. Thesis, University of California, Berkeley, California.

Washizu, K. (1982). *Variational Methods, in Elasticity and Plasticity*, 2nd Edn. Pergamon Press, New York.

Westmann, R. A. (1964). Layered systems subjected to asymmetric surface shears. *Proc. R. Soc. Edinb.* **66**, 140–149.

Wolf, J. P. and Darbre, G. R. (1984). Dynamic stiffness matrix of soil by the boundary-element method: conceptual aspects. *Earthquake Engng Struct. Dyn.* **12**, 385–400.

Zienkiewicz, O. C. (1977). *The Finite Element Method*, 3rd Edn. McGraw-Hill, U.K.

Zienkiewicz, O. C., Kelly, D. W. and Bettes, P. (1977). The coupling of the finite element method and boundary solution procedures. *Int. J. Numer. Meth. Engng* **11**, 355–375.